Pergamon

Journal of Structural Geology, Vol. 17, No. 4, pp. 461 to 474, 1995

0191-8141/95 $9.50+0.00

0191-8141(94)00071-9

Strain partitioning and crack-seal growth of chlorite–muscovite aggregates during progressive noncoaxial strain: an example from the slate belt of Taiwan

M. BROOKS CLARK and DONALD M. FISHER

Department of Geosciences, The Pennsylvania State University, University Park, PA 16802, U.S.A.

(*Received* 20 *August* 1993; *accepted in revised form* 7 *June* 1994)

Abstract—Chlorite–muscovite aggregates from the slate belt of southeastern Taiwan have an ellipsoidal geometry ($\sim k = 1$ on a Flinn diagram) with an aspect ratio $a:c$ ranging from about 7:1 to 12:1 and a crystallographic preferred orientation with the basal planes of the chlorite and muscovite at a high angle to the slaty fabric in the rock. The principal axes of the aggregates are approximately coaxial with the principal finite strain directions determined from fibrous pressure shadows. In cleavage parallel sections, straight fibers parallel to the downdip mineral lineation record plane strain. In cleavage perpendicular sections, however, pressure shadows have curved fibers that are consistent with W-directed thrusting. We propose a model in which the chlorite–mica aggregates grow syntectonically by cracking of detrital chlorite grains parallel to the basal planes and precipitation of secondary chlorite and mica in the open cracks. This model involves (1) rotation of pre-exiting detrital chlorite grains during progressive noncoaxial deformation, (2) cracking of these grains parallel to the basal plane when the (001) planes rotate into the incremental shortening field, with nucleation and growth of secondary chlorite and muscovite in the open microcracks. As the aspect ratio increases, the grains stabilize in orientation, with the long axes (normal to the basal planes) at a small angle to the shear direction. Extension normal to (001) is also accompanied by some shortening parallel to (001), but with an overall increase in size of the aggregates. The final grain size is controlled by the cumulative displacement associated with crack-seal events. Microprobe analyses of both detrital and secondary chlorite grains show distinct compositional differences within individual grains perpendicular to (001), particularly in the detrital grains, which we interpret as primary and secondary chlorite, consistent with a primary-and-secondary origin for the aggregates.

INTRODUCTION

Strain heterogeneity occurs at all scales, from regional variations in kinematics and strain magnitudes down to variations at the microscale (Bell 1981, Williams & Schoneveld 1981, Lister & Williams 1983). This heterogeneity occurs due to contrasts in material properties (e.g. bedding and grain boundaries) and may be enhanced during deformation due to strain softening or strain hardening. Bell *et al.* (1986) suggest that, at the scale of a thin section, an overall noncoaxial bulk deformation may be partitioned into areas of dominantly progressive shortening and areas of dominantly progressive shearing. Specifically, selvage zones which consist primarily of phyllosilicate grains aligned parallel to the foliation, accommodate the shearing component of the deformation, whereas the adjacent microlithons, consisting largely of quartz and feldspar, are dominated by progressive shortening (Bell 1981, Bell *et al.* 1986). Bell *et al.* (1986) further suggest partitioning may play an important role in the nucleation and growth of secondary minerals because fractures are likely to open in the zones of progressive shortening. These fractures provide easy access for fluids and therefore act as sites for the nucleation and growth of secondary minerals. In particular, fractures that form during the development of a crenulation cleavage are most likely to form parallel to the older fabric (S_1) in areas where S_1 is at a high angle to the crenulation cleavage (i.e. in the hinges of D_2 folds). Secondary minerals may nucleate on grains along the wall of the fracture and grow into the open crack (Bell *et al.* 1986). Other studies have also suggested that fractures are important for secondary mineral nucleation and growth (e.g. Voll 1960, White & Knipe 1978, van der Pluijm & Kaars-Sijpesteijn 1984, Lister *et al.* 1986).

In this paper, we discuss the growth of chlorite–muscovite aggregates from the slate belt of Taiwan (Fig. 1), and show that fracturing parallel to (001) is important for secondary growth of the aggregates. Numerous other examples of 'chlorite–muscovite aggregates' or 'chlorite–mica stacks' in low to intermediate grade slates have been described in the literature for a variety of different structural and kinematic settings (e.g. Sorby 1853, Behre 1933, Attewell & Taylor 1969, Beutner 1978, Weber 1981, Craig *et al.* 1982, Woodland 1982, 1985, van der Pluijm & Kaars-Sijpesteijn 1984, Gregg 1986, Beutner *et al.* 1988). Typically, the aggregates consist of stacks of chlorite and white mica and have a larger grain size than the surrounding matrix and a strong crystallographic preferred orientation with the basal planes at a high angle to the fabric in the rock. Despite the common occurrence of these chlorite–mica aggregates in slates, however, no consensus has been reached for their origin, except that fracturing parallel to the (001) planes may be an important mechanism for secondary mineral growth (Voll 1960, White & Knipe 1978, van der Pluijm & Kaars-Sijpesteijn 1984). Previous interpretations for the origin and growth of these aggregates generally fall into one of three categories, including: (1) primary origin (e.g. Beutner 1978), (2)

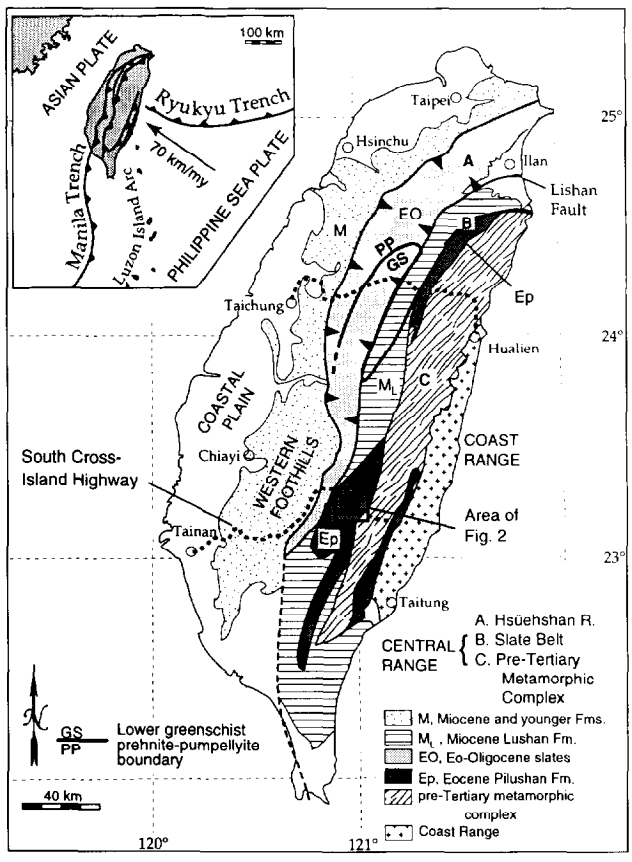

Fig. 1. Map showing the tectonic setting of Taiwan (inset) and map of Taiwan showing the major lithotectonic units. The box shows the location of Fig. 2. After Chen (1984) and Ho (1986). Inset after Davis *et al.* (1983).

primary and secondary origin (e.g. Voll 1960, White & Knipe 1978, van der Pluijm & Kaars-Sijpesteijn 1984, Beutner *et al.* 1988), or (3) secondary origin (e.g. Behre 1933, p. 180, Weber 1981). Observations of chlorite–mica aggregates from the slate belt of Taiwan, in conjunction with analyses of fibrous pressure shadows in the matrix, suggest that strain is locally partitioned around the chlorite–mica aggregates such that noncoaxial deformation in the matrix is accompanied by coaxial extension and crack-seal deformation within the aggregates.

GEOLOGIC SETTING

Taiwan is an active orogenic belt situated on the boundary between the Eurasian and Philippine Sea plates and is a result of the collision between the Luzon island arc and the Asian continental margin (Ho 1975, 1986, 1988). In general, Taiwan can be divided into five major lithotectonic units, including, from west to east, the Coastal Plain, the Western Foothills, the Hsüehshan Range, the Central Range, and the Coastal Range (Fig. 1). Except for the Coastal Range, which represents the accreted volcanic arc and forearc basin sediments, both the age and metamorphic grade tend to increase progressively from west to east across the island (Chen 1984, Ho 1986). The Central Range exposes the oldest rocks in Taiwan and is divided into two belts, including the Tananao Schist, a polydeformed pre-Tertiary metamorphic complex in the east, and a massive sequence of Eocene slates and metasandstones in the west (Pilushan Formation). The metamorphic complex consists of a variety of rock types, including marble, phyllite, quartz–mica schist, greenstone and granofels (Stanley *et al.* 1981), and is interpreted to represent Asian continental basement (Ho 1975, 1986, Ernst *et al.* 1988). The Pilushan Formation is a sedimentary cover sequence unconformably overlying the Tananao Schist, although the unconformity may have been reactivated as a fault during the collision (Ho 1986, 1988).

Field mapping was conducted along the South Cross-Island Highway between Yakou Hostel and the contact with the Tananao Schist (Fig. 2). Structurally, the Pilushan Formation is characterized by a well-developed slaty cleavage (S_1) and a mineral lineation which is approximately downdip on the cleavage planes (Fig. 2). Throughout the slates, bedding is parallel or subparallel to cleavage and both dip moderately to the southeast in the western part of the field area. Where there is an angular relationship between bedding and cleavage, cleavage is generally several degrees steeper than bedding. This parallelism or near parallelism is attributed to large amounts of angular shear parallel to lithologic layering (Stanley *et al.* 1981, and as discussed below). In the east, S_1 is folded by D_2 and D_3 but generally dips steeply to the northwest (Fig. 2, e.g. samples SX-68 and SX-70).

Compositionally, the slates consist of chlorite, quartz, muscovite and minor framboidal pyrite with average grain sizes on the order of 10 μm or less. The chlorite occurs in three distinct forms, including primary (detrital) grains, secondary grains defining the S_1 foliation, and large aggregate grains composed of chlorite (more than 60%), muscovite (less than 30%), and relatively minor quartz. The detrital chlorites are found only in some of the less deformed and coarser-grained lithologies from the westernmost part of the field area (Fig. 2, sample SX-4). They are characterized by a platy habit with dimensions in the order of 150–200 μm parallel to the basal planes and slightly shorter normal to the basal planes (Fig. 3c). Sample SX-4 was taken from the hinge of a very tight mesoscale fold and is one of the few examples where cleavage is at a high angle to bedding, with the cleavage-bedding angle ranging from approximately 40° to 90°. In this sample, the detrital chlorite grains have a very well developed crystallographic preferred orientation with the basal planes nearly orthogonal to cleavage (dipping ~30° to the west in a geographic reference frame).

The chlorite–mica aggregate grains found in the highly deformed slates to the east are generally much larger than grains in the surrounding matrix, with lengths in the order of 500–2000 μm normal to the basal planes and 50–200 m parallel to the basal planes. These grains also show a strong crystallographic preferred orientation.

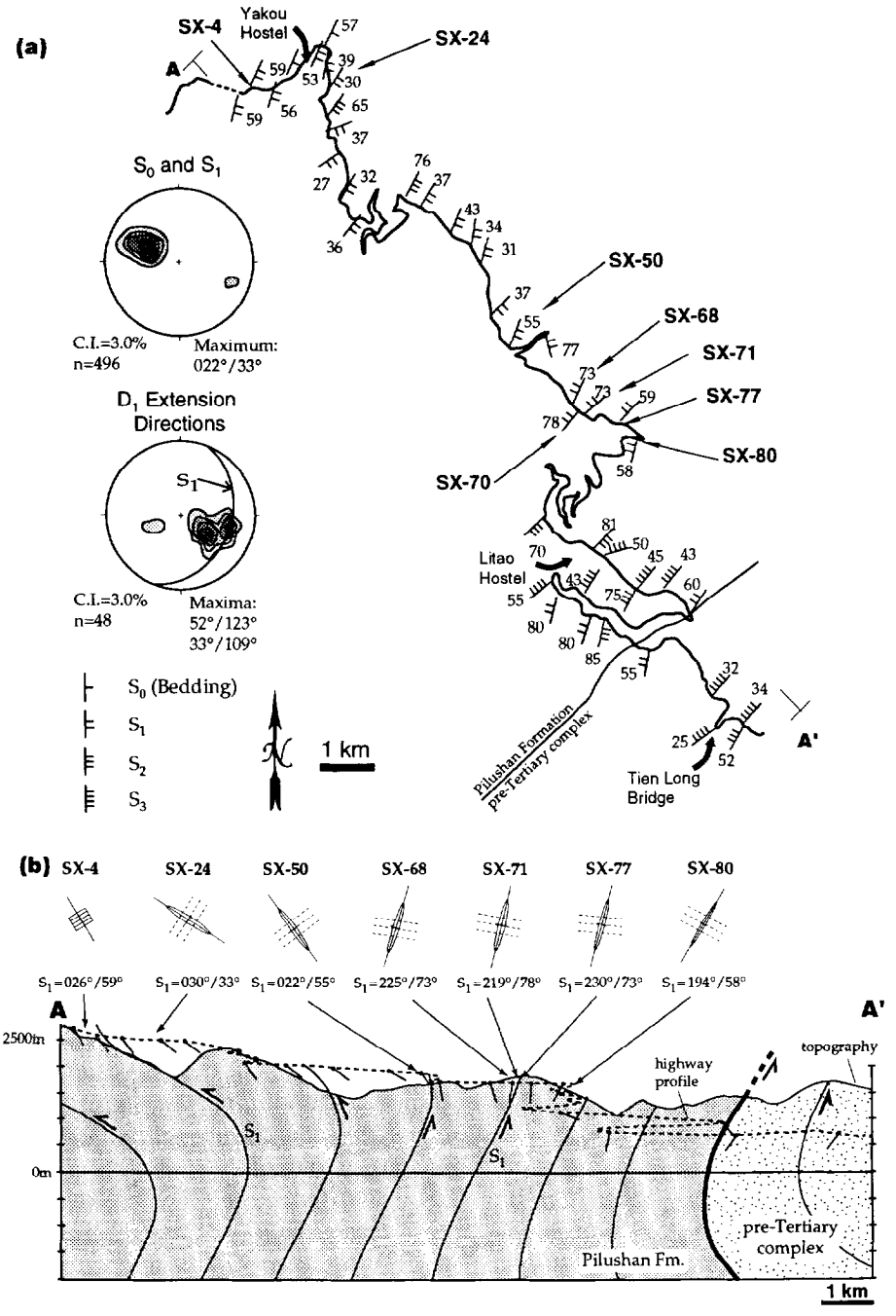

Fig. 2. (a) Map showing sample locations and structural data for slates of the Pilushan Formation. Location given in Fig. 1. (b) Simplified cross-section showing the trace of cleavage along section A–A'.

KINEMATICS OF DEFORMATION IN THE MATRIX

Syntectonic fibrous overgrowths in pressure shadows adjacent to a rigid object record displacement paths between initially adjacent points in a deformed rock and can therefore be used to establish the kinematics of matrix deformation in the vicinity of rigid grains (Durney & Ramsay 1973, Wickham 1973, Ramsay & Huber 1983, Beutner & Diegel 1985, Ellis 1986). Durney & Ramsay (1973) and Ramsay & Huber (1983) assume that fibers grow parallel to the incremental extension direction. Pressure shadows with curved fibers therefore record a rotation of the incremental extension direction relative to an external reference frame (e.g. the final orientation of bedding or cleavage). This rotation may reflect: (1) spin of the rock body through the incremental extension direction, or (2) noncoaxial strain with progressive rotation of the fibers relative to a fixed internal reference frame such as the incremental stretching direction or shear zone boundaries.

Fibrous quartz–chlorite overgrowths in pressure shadows adjacent to large quartz grains and framboidal pyrite grains are relatively abundant in slates from the Pilushan Formation. To characterize the three-dimensional geometry of the pressure shadows, two thin

sections were cut from each sample—one parallel to cleavage (*XY* section), and one perpendicular to cleavage and parallel to the downdip mineral lineation (*XZ* section, viewed toward the northeast). This mineral lineation, which is observable throughout most of the slates, is parallel to the maximum dimension of overgrowths and is representative of the direction of maximum finite stretch. In *XY* sections, pressure shadows have straight fibers parallel to the approximately downdip mineral lineation, indicating northwest extension (Fig. 3a). Straight, downdip fibers in the cleavage-parallel sections are consistent with plane strain without along-strike extension or shortening (parallel to *Y*).

In *XZ* sections, pressure shadows have curved fibers (Fig. 3b) reflecting a rotational strain history. To determine the correct sense of rotation, however, it is necessary to independently establish the direction of fiber growth. Fibers may grow from the host toward the matrix, so that the youngest portion of the fibers is farthest from the host (syntaxial growth), or from the matrix toward the host, so that the youngest overgrowths are nearest the host (antitaxial growth). Antitaxial growth is most common when the composition of the fibers is similar to the matrix and different from the host, for example quartz–chlorite fibers adjacent to framboidal pyrite grains (Durney & Ramsay 1973, Ramsay & Huber 1983, Beutner & Diegel 1985, Ellis 1986, Fisher 1990, Clark *et al.* 1993). Antitaxial growth in the pyrite pressure shadows from the Pilushan Formation is also supported by the observation that overgrowths adjacent to large quartz grains have the opposite sense of curvature. Fibers in the quartz pressure shadows are in optical continuity with the host and are therefore syntaxial. Fibers in both quartz and pyrite pressure shadows therefore record a counterclockwise rotation of the rock relative to a fixed extension direction through time (looking north), or alternatively, a bulk counterclockwise angular shear (Fig. 3b). Of the two possible interpretations for pressure shadows with curved fibers, we prefer the interpretation that fiber curvature is related to bulk angular shear for two reasons. Firstly, a counterclockwise rotation of the rocks through a vertical incremental extension direction is inconsistent with the regional eastward dip (in the western part of the area). Secondly, independent kinematic indicators such as folds and asymmetric boudins have a sense of asymmetry consistent with top-to-the-northwest angular shear (Stanley *et al.* 1981).

DESCRIPTION OF CHLORITE–MUSCOVITE AGGREGATES

The chlorite–muscovite aggregates are composed primarily of chlorite, but in many cases contain abundant muscovite and minor quartz, where relatively large chlorite books are separated by thinner muscovites (Fig. 4). Inclusions of any matrix grains within the aggregates are notably absent, indicating that growth did not involve replacement of the matrix (e.g. the biotite porphyroblasts of Lister *et al.* 1986). Two principal sections were cut for each sample as described earlier (one parallel to cleavage, one perpendicular to cleavage and parallel to the stretching lineation). In both sections, the aggregates are sub-elliptical indicating an overall ellipsoidal geometry in three dimensions, with the average orientation of the principal axes of the ellipsoid closely corresponding to the principal strain axes (i.e. the long axis is parallel to the mineral lineation in *XY* sections, the intermediate axis is perpendicular to the mineral lineation, and the short axis is nearly perpendicular to cleavage).

To characterize the geometries of the aggregates in the two principal sections, we used a digitizing tablet to digitize up to 50 points on the edge of each aggregate, then calculated a root mean square best-fit ellipse using the algorithm of Erslev & Ge (1990). In this paper, we refer to the chlorites in a reference frame where x is perpendicular to the basal planes, and y and z are parallel to the basal planes (parallel to Y and Z, respectively). The notation a, b, and c refer to the maximum, intermediate, and minimum axes of the aggregates, respectively. Figure 5(a) shows the present geometry of the aggregates on a Flinn (1962) diagram. The aggregates generally plot near the $k = 1$ line, but may be slightly prolate or slightly oblate.

Undeformed micas typically have a platy habit with the length parallel to the basal planes being longer than the length normal to the basal planes (Woodland 1985). Beutner (1978) reports an average aspect ratio 2.67:1 for detrital chlorites in uncleaved pelites from the Martinsburg Slate of the eastern United States. In sample SX-4, which contains relatively undeformed detrital chlorites, the average aspect ratio is in the order of 1.3–1.5 to 1 measured in *XZ* sections (Fig. 3c). Moreover, the length in two orthogonal directions parallel to the basal planes should on average be approximately equal ($x < y \cong z$) and undeformed phyllosilicates should plot near the $k = 0$ axis of a Flinn diagram.

One of the most striking features of the aggregates is the strong crystallographic preferred orientation with the (001) planes are at a high angle to S_1 viewed in *XZ* sections (subparallel to c) and approximately parallel to b in *XY* sections. Although some of the aggregates have deformed internally by slip along the basal planes, in most cases, the amount of reorientation of the (001) planes due to internal deformation is small. Rose diagrams showing the long axes of the calculated best-fit ellipses and the orientation of the basal planes are shown in Figs. 6(a)–(f) for *XY* sections and Figs. 6(g)–(l) for *XZ* sections. On average, the basal planes are oriented slightly clockwise from the short axis of the ellipse (less than ~10°). The average geometries and orientations of the aggregates in an absolute reference frame are shown schematically on the cross-section (Fig. 2b). In the western part of the area where cleavage dips moderately to the southeast, the (001) planes of the aggregates dip moderately to the northwest (Fig. 2b, samples SX-24 and 50).

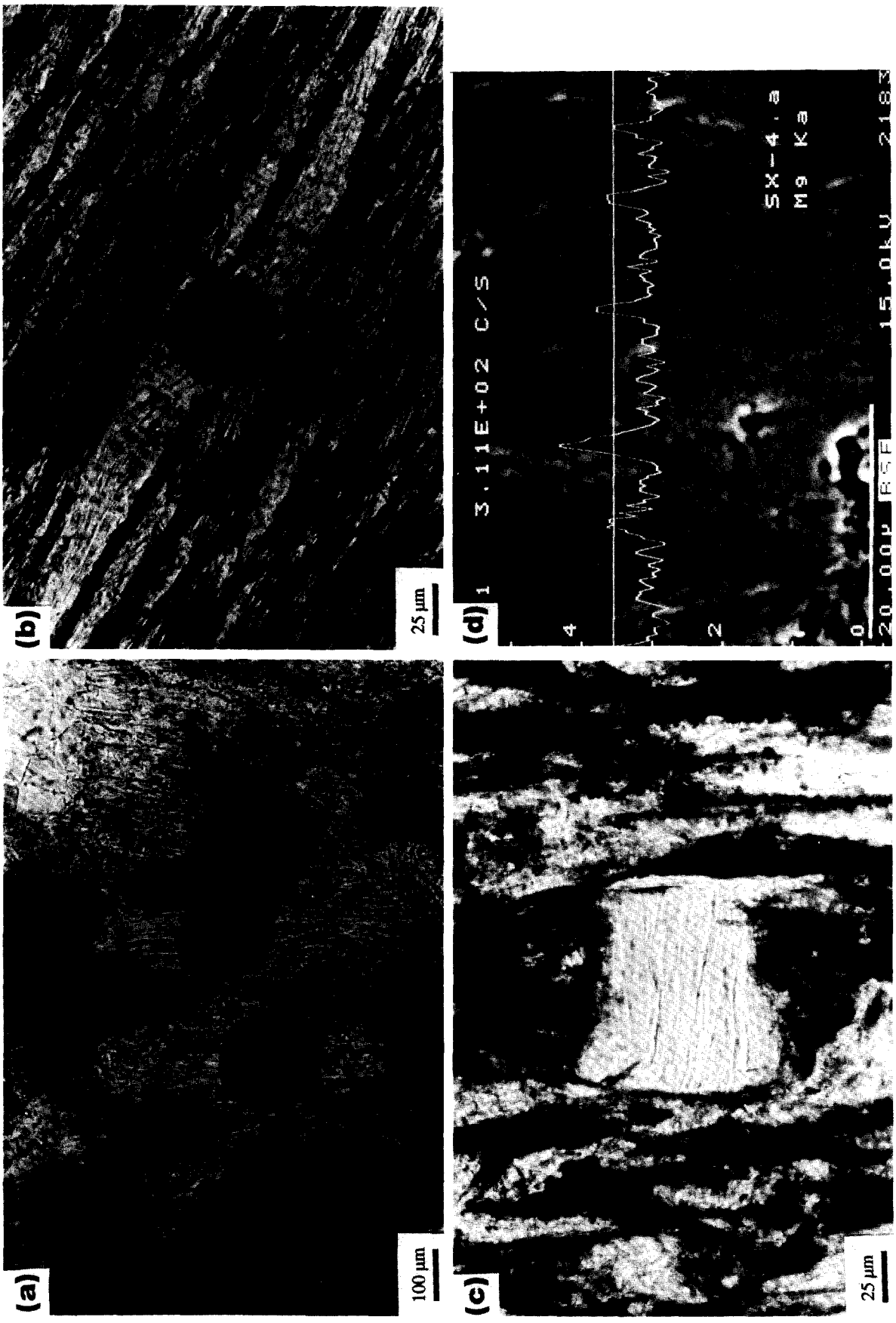

Fig. 3. (a) Pyrite pressure shadows viewed in a cleavage parallel section (sample SX-5). (b) Pyrite pressure shadow viewed in a cleavage perpendicular thin section (sample SX-22). (c) A moderately deformed detrital chlorite–muscovite grain from sample SX-4. (d) Backscatter SEM-photomicrograph of the same grain showing the typical light and dark banding of chlorite with different compositions (superimposed graph shows the K_α values for Mg).

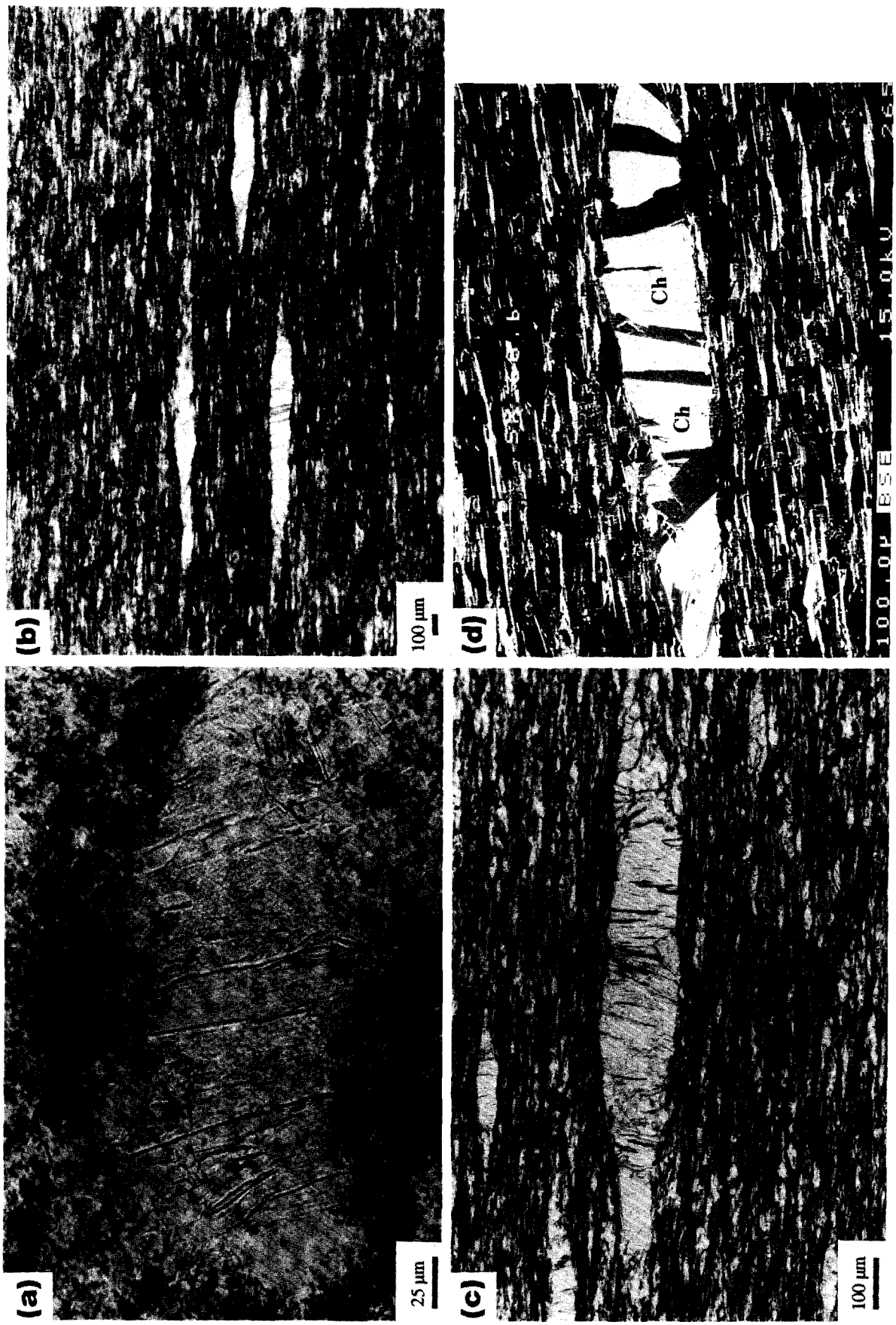

Fig. 4. Photomicrographs of highly deformed chlorite (Ch)–muscovite (M) aggregates (a) viewed in *XY* section (SX-77), (b) viewed in *XZ* section (SX-70), (c) viewed in *XZ* section (grain SX-68a), and (d) backscatter SEM-photomicrograph of grain SX-68b in *XZ* section.

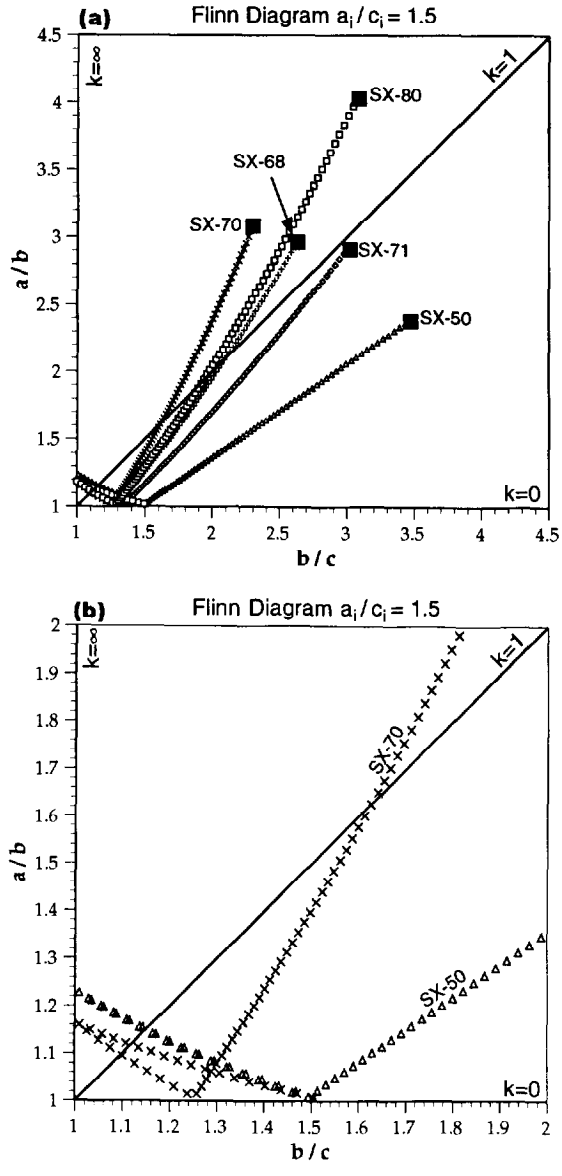

Fig. 5. Flinn diagrams showing the calculated path the chlorite–mica aggregates follow beginning with an initial geometry of $a_i/c_i = 1.5$ (see text), where (a) shows the average final geometries for five samples, and (b) shows the details of the paths near the origin.

MICROPROBE ANALYSIS OF CHLORITES

The compositions of detrital chlorites, secondary chlorites, and chlorite–mica aggregates were analyzed on an electron microprobe (Table 1). The detrital grains, denoted SX-4a and SX-4b, are from sample SX-4 in the westernmost part of the field area (see Fig. 2 for sample location). Under backscatter, these detrital chlorite grains show a distinct light and dark banding parallel to (001) (Fig. 4d), with the dark bands approximately 2 μm wide and the lighter bands on the order of 10–20 μm. Analyses SX-4a.1 and SX-4b.1 are from within the lighter bands; SX-4a.2 and SX-4b.2 are within the dark bands (Table 1). These bands have distinctly different compositions, with the dark bands having a higher MgO/FeO ratio (Fig. 7).

Analysis SX-68c is from a secondary chlorite grain that is parallel to the foliation (sample SX-68). This grain is similar in composition to the higher Mg chlorite in the dark bands of the detrital grain.

Two chlorite–mica aggregates from sample SX-68 were also analyzed. The first, denoted SX-68a (Fig. 4d), includes five points selected by hand. The second, denoted SX-68b, includes 17 approximately evenly spaced points along a transect across the entire aggregate, 14 of which were chlorite. These analyses show a relatively limited range of compositions, with many of the points having an Mg number of approximately 0.45, similar to the composition of the secondary grain. The variations in composition within the aggregate represent differences in the weight percent of Fe on the order of 0.7% and may reflect submicroscopic interlayers with different compositions (Li *et al.* 1994).

DISCUSSION

Deformation mechanisms and kinematics of aggregate growth

The coaxiality of the a, b and c axes of the aggregates with the X, Y and Z axes of the finite strain ellipsoid, respectively, suggests that the external geometry of the aggregates is related to D_1. Additionally, zones of insoluble residue along edges of the aggregates that face the shortening direction indicate that the aggregates were present during D_1. Any model for growth and/or deformation of these aggregates must not only produce the observed external geometry, but also account for the crystallographic preferred orientation such that (001) planes are aligned subparallel to the short axes of the aggregates (i.e. suborthogonal to S_1). Moreover, the strain path must map the grain shape from an approximately $k = 0$ geometry to the final observed geometry of the aggregates. Three possibilities include: (1) pressure solution of material along the edges of pre-existing chlorite–muscovite grains (e.g. Beutner 1978), (2) intracrystalline (crystal-plastic) deformation of pre-existing detrital chlorite grains or early-formed aggregates, or (3) microfracturing of initially platy chlorites or white micas and infilling of the microcracks with secondary minerals (Voll 1960, White & Knipe 1978, van der Pluijm & Kaars-Sijpesteijn 1984). Each of these possibilities is discussed below.

(1) Beutner (1978) describes large chlorite grains from the Martinsburg Slate, New Jersey, U.S.A. These grains are interpreted as detrital chlorites and show both a strong grain-shape and a crystallographic preferred orientation, with the long axis approximately parallel to cleavage. Beutner (1978) attributes the crystallographic preferred orientation to a primary bedding fabric and suggests that the grains deformed primarily by pressure solution corrosion along edges parallel to the foliation in the rock, with little or no systematic rotation of the grains. Assuming that the chlorite grains initially had a platy habit typical of mica and chlorite ($x < y \cong z$), pressure solution alone cannot produce the final grain geometries observed in the samples from Taiwan.

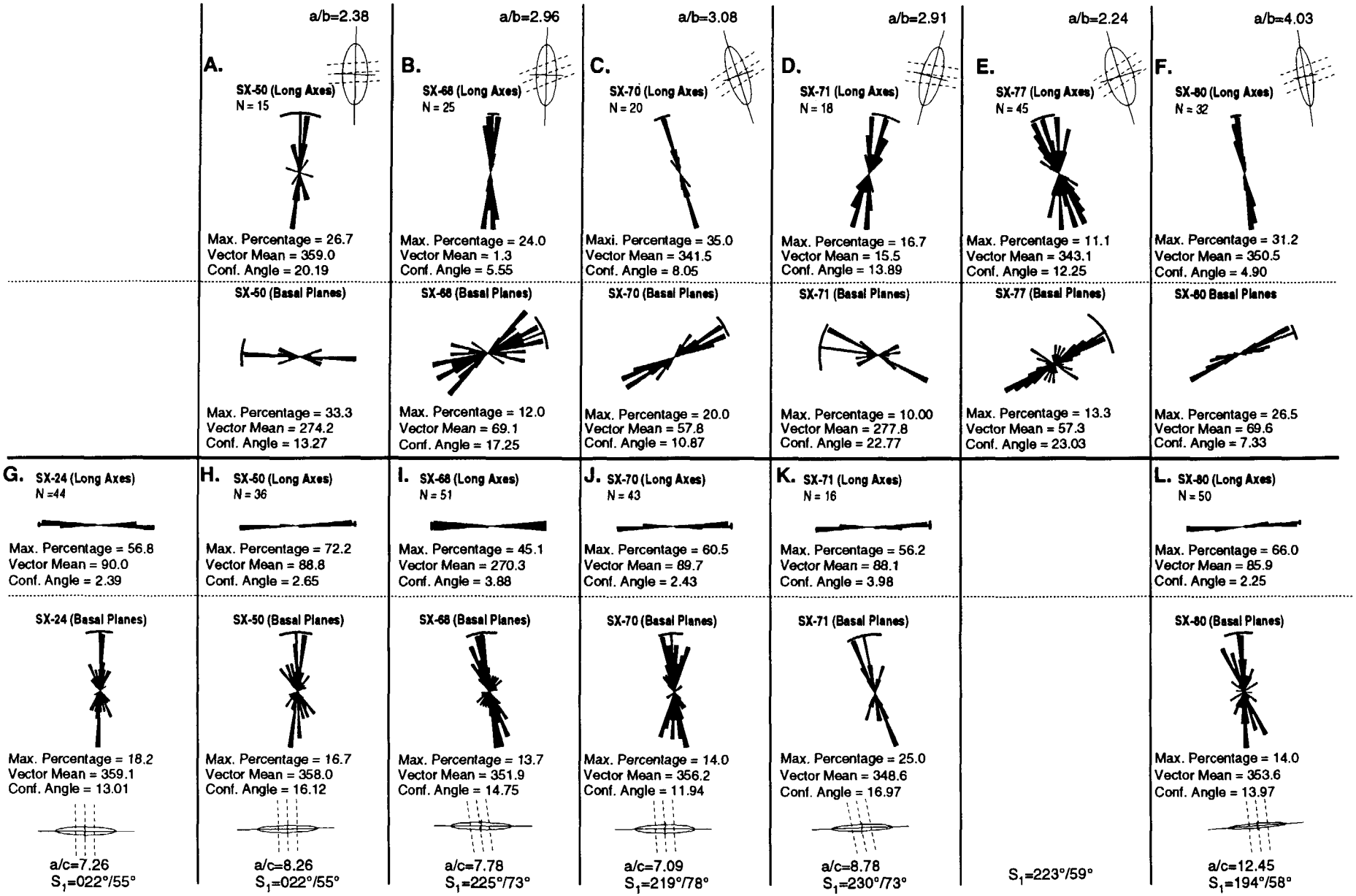

Fig. 6. Rose diagrams showing the orientation of the long axes of the calculated best-fit ellipse and the basal plane orientation in S_1 parallel (a)–(f) and S_1 perpendicular (g)–(k) sections. The XY sections are shown in a reference frame where the strike of S_1 is horizontal; XZ sections are shown in a reference frame where the trace of cleavage is horizontal. a/b and b/c are the average axial ratios of the aggregates in XY and XZ sections, respectively, and N is the number of aggregates measured. The vector mean is the average orientation, and the confidence angle shows the range of orientations that includes 95% of the data. Note that the radial scale is different for each rose diagram; the maximum percentage is the percentage of data points represented by the longest bar. The ellipses show the average ellipticity and orientation of the aggregates.

Table 1. Microprobe data for all chlorite analyses, including two detrital chlorite grains (SX-4a and b), a secondary chlorite grain in the matrix (SX-68c), and two chlorite–muscovite aggregates from the high strain zone (SX-68a and b)

	SX-68a.1	SX-68a.2	SX-68a.4	SX-68a.5	SX-68a.6	SX-68b.1	SX-68b.2	SX-68b.3
SiO_2	22.893	23.318	24.357	24.685	24.301	24.242	24.752	24.287
Al_2O_3	22.318	22.267	22.590	22.647	22.202	22.837	22.222	22.877
MgO	12.314	12.200	12.471	12.533	12.657	12.174	12.263	12.489
FeO	28.055	28.442	28.396	28.336	27.724	26.783	26.980	26.922
Na_2O	0.000	0.019	0.000	0.010	0.009	0.004	0.019	0.000
K_2O	0.016	0.000	0.002	0.009	0.041	0.000	0.035	0.018
Total	85.596	86.246	87.816	88.220	86.934	86.040	86.271	86.593
Mg-number	0.439	0.433	0.439	0.441	0.449	0.448	0.448	0.453

	SX-68b.4	SX-68b.5	SX-68b.7	SX-68b.8	SX-68b.10	SX-68b.11	SX-68b.12	SX-68b.13
SiO_2	24.212	25.049	24.351	24.362	23.934	24.272	24.420	24.262
Al_2O_3	22.598	22.741	22.796	22.452	23.068	22.747	22.805	22.444
MgO	12.285	12.324	12.397	12.288	11.560	12.379	12.227	11.936
FeO	27.251	27.223	27.116	27.149	27.522	27.029	27.251	27.250
Na_2O	0.000	0.013	0.003	0.008	0.013	0.012	0.000	0.005
K_2O	0.011	0.011	0.025	0.042	0.029	0.010	0.027	0.030
Total	86.357	87.361	86.688	86.301	86.126	86.449	86.730	85.927
Mg-number	0.446	0.447	0.449	0.447	0.428	0.449	0.444	0.438

	SX-68b.15	SX-68b.17	SX-68b.18	SX-68c	SX-4a.1	SX-4a.2	SX-4b.1	SX-4b.2
SiO_2	24.649	23.742	24.888	24.296	24.491	25.917	25.267	26.155
Al_2O_3	22.917	22.263	22.662	22.709	22.248	20.100	21.991	20.415
MgO	11.844	11.936	12.485	12.271	10.020	13.412	10.608	12.643
FeO	27.681	26.908	26.877	26.790	29.947	27.331	29.933	27.554
Na_2O	0.000	0.011	0.000	0.000	0.000	0.004	0.018	0.007
K_2O	0.027	0.030	0.043	0.022	0.007	0.000	0.094	0.060
Total	87.118	84.890	86.955	86.088	86.713	86.764	87.911	86.834
Mg-number	0.433	0.442	0.453	0.449	0.374	0.467	0.387	0.450

However, pressure shadows record no evidence for shortening or extension parallel to Y (plane strain), therefore, the width of the chlorite–mica aggregates parallel to Y probably approximates the initial length parallel to the basal planes. Unless the original grains had an unusual geometry where the long axis of the grains was normal to the basal planes, dissolution (and local volume loss) along edges of the grain parallel to the foliation cannot produce the final geometries ($x \gg y > z$).

(2) Intracrystalline deformation may be accommodated either by recrystallization and grain size reduction, or slip along the basal planes. Recrystallization does not appear to be an important mechanism, however, because most grains span the entire width of the aggregate and there is no evidence for localized deformation zones (Vernon 1977) or grain size reduction along zones at an angle to the basal planes. Additionally, slip parallel to the basal planes would result in a crystallographic preferred orientation with (001) oriented at a small angle to the fabric in the rock and subparallel to

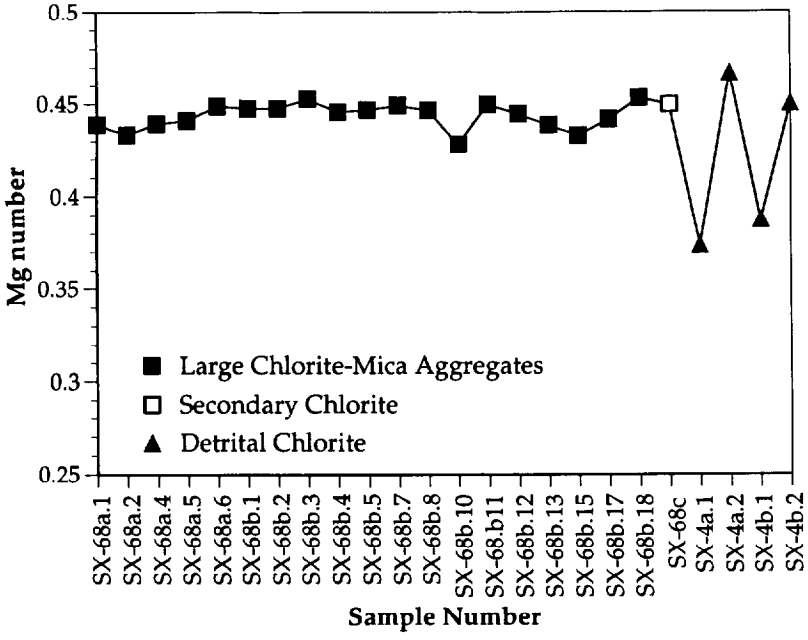

Fig. 7. Plot of Mg number vs analysis number. See text for explanation.

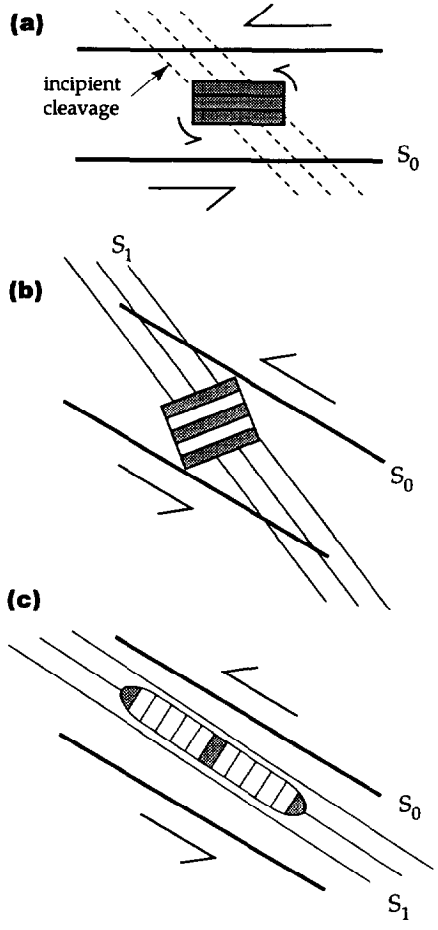

Fig. 8. Schematic diagram showing bedding–cleavage-aggregate relationships through time.

the long dimension of the aggregates. Generally, the amount of slip along the basal planes is small in all but a few of the chlorite–muscovite aggregates and the basal planes are at a high angle to the foliation. Thus, this mechanism cannot explain the preferred orientation of the basal planes at a high angle to S_1. Although there is some evidence for a small amount of slip parallel to (001), intracrystalline deformation is not thought to be significant.

(3) The third mechanism, involving microfracturing within and adjacent to (Voll 1960, White & Knipe 1978, van der Pluijm & Kaars-Sijpesteijn 1984, Lister *et al.* 1986) pre-existing chlorites and precipitation of secondary chlorite and mica in the open microcracks, provides the best interpretation to explain both the geometry and preferred orientation of the chlorite–muscovite aggregates. The detrital chlorites observed in less deformed rocks to the west are a likely candidate for the pre-existing chlorites, and the presence of (001)-parallel bands within the detrital grains of chlorite that is similar in composition to secondary chlorite in samples to the east supports the idea that the detrital grains undergo extension orthogonal to (001), with precipitation of secondary minerals within distinct bands. As envisaged, this process involves two stages: (1) Detrital chlorites ($x < y \cong z$) rotate in response to bulk shear (Fig. 8a). These detrital grains are interpreted to have a primary preferred orientation with (001) parallel to bedding (e.g. Beutner 1978, Craig *et al.* 1982, Woodland 1982, 1985, van der Pluijm & Kaars-Sijpesteijn 1984). The grains are initially oriented with the basal planes at a moderate angle to the incremental shortening direction and therefore behave relatively rigidly during this stage. (2) Once x is within the incremental extension field, the detrital chlorites begin to deform by fracturing parallel to the basal planes, resulting in extension normal to the basal planes. In this orientation, the aggregates behave passively because of the negligible tensile strength of chlorite normal to the basal planes. Both secondary chlorite and muscovite nucleate on the pre-existing detrital chlorites along the walls of the crack and grow, filling in the open crack until the process is repeated by the opening of a new fracture (Fig. 8). Secondary chlorite and muscovite nucleate on the pre-existing grains, maintaining crystallographic continuity with the precursor detrital chlorite.

Stage 1: *rotation of detrital grains.* Previous studies of chlorite–mica aggregates have resulted in several alternative interpretations for rotation of the aggregates during deformation. These interpretations generally fall into one of three categories, including (1) little or no rotation (Beutner 1978), (2) no rotation with respect to bedding (Craig *et al.* 1982, Woodland 1982, 1985), and (3) mechanical rotation toward parallelism with cleavage (van der Pluijm & Kaars-Sijpesteijn 1984). Beutner (1978) shows that detrital chlorite grains undergo little or no systematic rotation with respect to a geographic reference frame during passive folding and used the orientation of (001) to determine the original orientation of bedding. Craig *et al.* (1982) and Woodland (1982, 1985) show evidence that the aggregates rotate with respect to a geographic reference frame, but maintain approximate parallelism with bedding during folding. Woodland (1982) concludes that, in all but a few samples, the aggregates show no evidence for rotation toward cleavage. In contrast, van der Pluijm & Kaars-Sijpesteijn (1984) show evidence that the aggregates rotate toward cleavage on the limbs of folds. This rotation is interpreted as a rigid body rotation and is attributed to noncoaxial strain histories on the limbs of folds.

Bell & Johnson (1989) show that foliations preserved in porphyroblasts tend to have subvertical or subhorizontal orientations and suggest that the porphyroblasts undergo no rotation during deformation. Bell *et al.* (1992) further support this idea with data from a variety of localities showing vertical and horizontal truncations. Assuming an initial bedding-parallel preferred orientation for the chlorite–mica aggregates from Taiwan, however, a nonrotation model predicts that (001) would remain roughly horizontal during passive rotation of bedding and cleavage formation. Presently, (001) are on average normal to both bedding and cleavage, requiring a relative rotation between (001) and bedding of ~90°. In the western part of the field area where D_2 and D_3 folds are absent, bedding dips approximately 30–60° southeast (Fig. 2) as a consequence of clockwise (look-

ing north) tilting during thrusting. The chlorite–mica aggregates from this area (samples SX-4, 24 and 50), however, dip to the northwest approximately 45–60°, consistent with a counterclockwise rotation. Therefore, the present orientation of the (001) planes in aggregates is best explained by early rotation during northwest-directed thrusting.

Stage 2: crack-seal growth of the aggregates. The observation that the long axis of the chlorite–mica aggregates is almost normal to the (001) planes (Figs. 6g–l) is of particular importance because it suggests that extension occurred normal to the basal planes (mode I fracturing) rather than by mixed-mode or shear fracturing with a component of displacement parallel to the basal planes (antithetic shearing). If mixed mode fracturing were important, the basal planes would continue to rotate toward parallelism with the shear plane and approach parallelism with the long axis. Mixed-mode fracturing is clearly not consistent with the observations, suggesting a high degree of strain partitioning between the chlorite–mica aggregates and the surrounding matrix. Whereas deformation in the matrix is noncoaxial, the aggregates deform by coaxial extension normal to (001) and shortening parallel to (001), i.e. the noncoaxial strain in the matrix is locally partitioned into coaxial stretching and spin in the aggregates (e.g. Lister & Williams 1983). The spin decreases as the long axis of the aggregate approaches parallelism with the shear direction. Because extension occurs normal to (001), the longest dimension of the aggregates is normal to the basal planes for moderate to large strains, so the aggregates stabilize in orientation with the long axis parallel to cleavage and (001) normal to cleavage.

Light and dark bands in detrital chlorite grains from sample SX-4 have two distinct chemical compositions. The higher Mg end-member in the (001)-parallel bands is similar in composition to secondary grains and is interpreted to be secondary. The fact that these bands are parallel to (001) is consistent with fracturing of the detrital grains parallel to (001) with precipitation of secondary chlorite in the open cracks. Large chlorite–mica aggregates are dominated by the higher Mg chlorite, suggesting significant secondary growth of the aggregates.

Chlorite–mica aggregate geometries and strain paths

Detrital or undeformed micas typically have a platy habit ($x < y = z$); therefore, any viable strain path must map the aggregates from a $k = 0$ geometry to approximately $k = 1$ ellipsoids (Fig. 5). The resulting changes in the grain shape can be represented as continuous paths on a Flinn (1962) diagram. Two end-member strain paths we will consider are pure volume gain by extension normal to (001), and volume constant strain accommodated by extension normal to (001) accompanied by an equal amount of shortening in one direction parallel to (001). The paths shown on the Flinn (1962) diagram represent the changes in shape of the aggregates and we emphasize that the strain paths discussed here refer only to the chlorite–mica aggregates and not to the rock as a whole. Although deformation of the rock is noncoaxial, deformation of the aggregates is roughly coaxial because extension always occurs normal to the basal planes.

Starting with a chlorite grain that initially has a platy habit with dimensions $x < y = z$ (Fig. 9, point m), extension parallel to x would cause the grain to become less oblate and subsequently more prolate (Fig. 9, black curve, points m–n–o); such deformation would not result in different lengths for y and z ($x > y = z$). Therefore, pure volume gain due to fracturing parallel to the basal planes cannot produce the final observed geometries. Alternatively, starting with a chlorite with the same geometry (Fig. 9, point m), volume constant deformation results in a slightly more complicated history which ultimately produces an oblate ellipsoid. Now it is assumed that extension parallel to x is accommodated by an equal amount of dissolution parallel to z, with no extension or shortening parallel to y. In this case, the aggregates follow the path represented by the dashed curve (Fig. 9, points m–n′–o′–p′), ultimately producing an oblate geometry; the geometries of the grains at each point are shown schematically (Fig. 9). Thus, starting with a grain with a platy habit, volume constant deformation will always result in an oblate ellipsoid provided the amount of deformation is large enough to cause x to become the longest dimension of the aggregate. Again, this strain path cannot map the aggregates from their initial to final geometries.

Now consider deformation intermediate between pure volume gain and volume-constant strain, involving extension parallel to x and shortening parallel to z: treating the deformation of the aggregates as coaxial, there are three independent variables that define the final aggregate geometry: the maximum principal stretch s_1, the minimum principal stretch s_3, and the initial geometry of the precursor chlorite grains (a_i/c_i). By constraining any two of these three variables, we can show the changes in shape of an initially undeformed mica grain ($x < y = z$) on a Flinn diagram as a function of the third for a coaxial strain history.

Because pressure shadows record no independent evidence for extension or shortening parallel to Y ($s_2 = 1$), the y dimension of the aggregates is assumed to approximate the original length parallel to the basal planes ($y_f = y_i = z_i$). The final length parallel to (001) is z_f, so

$$s_3 = z_f/y_i, \tag{1}$$

or using the axial ratios shown in Fig. 6,

$$s_3 = (a/b)/(a/c). \tag{2}$$

Given the range in values for the initial aspect ratio a_i/c_i discussed earlier (~1.3–2.5:1), we can calculate the value of s_1 required to deform the grains to the final geometries. To show the evolution of the geometry on a Flinn (1962) diagram, the deformation is divided into 100 equal increments where the maximum and minimum incremental stretches are $(s_1)_i = (s_1)^{0.01}$ and $(s_3)_i =$

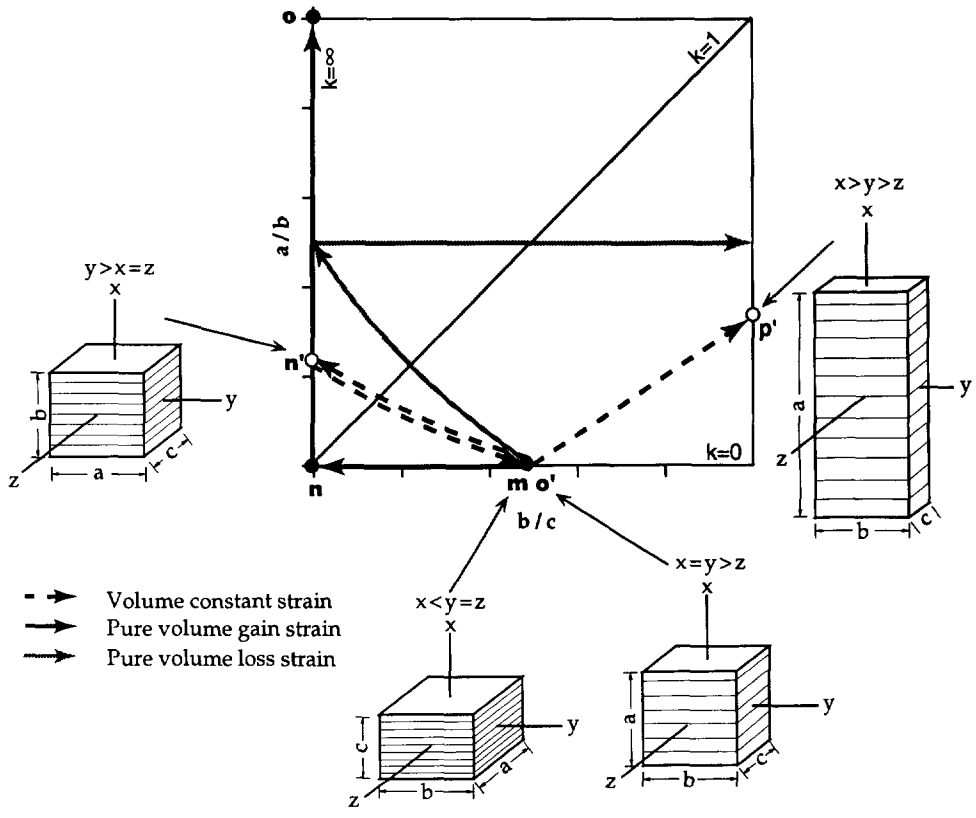

Fig. 9. A schematic Flinn diagram showing the paths that a grain with initial dimensions $x = y > z$ (point m) would follow for several different strain paths, including pure volume-gain strain, volume-constant strain, and pure volume-loss strain (grey curve), where the extension direction is parallel to x and the shortening direction is parallel to z. For pure volume gain, the grain follows the path m–n–o (solid line), resulting with a prolate geometry. For volume constant strain, the grain follows the path m–n'–o'–p' (dashed line), ultimately resulting in an oblate geometry. The block diagrams schematically show the axial ratios of the grain at points m, n', o' and p'.

$(s_3)^{0.01}$, respectively. Because each increment is coaxial with earlier increments, the length of the chlorite grain parallel to x is $x_{i+1} = x_i(s_1)_i$ and the length parallel to z is $z_{i+1} = z_i(s_3)_i$ after each increment.

Table 2 shows the measured final aspect ratios a_f/c_f for the aggregates and the calculated values for s_1 and volume change Δ for grains having initial aspect ratios a_i/c_i of 1.25, 1.5, 2.0 and 2.5. In almost all cases, the deformation involves an overall volume gain ($\Delta > 0$) at the scale of an individual grain. This volume-gain strain is consistent with our interpretation that growth of the aggregates involves pressure solution at the cleavage-parallel edges and cracking parallel to the basal planes, with precipitation of secondary chlorite and muscovite in the cracks. Figures 5(a) & (b) show the paths that the aggregates follow from their initial to final geometries on a Flinn (1962) diagram for an initial aspect ratio of 1.5. Deformation intermediate between pure volume gain and volume-constant strain can therefore lead to either prolate or oblate ellipsoids, depending on whether the slope of the linear segment of the path (e.g. Fig. 9, points o'–p') is greater than or less than unity. The slope of this line is a function of the initial aspect ratio of the chlorite grains and the ratio s_1/s_3.

CONCLUSIONS

We have outlined a kinematic model to explain the growth of chlorite–muscovite aggregates from Taiwan during noncoaxial strain history. This model involves rigid rotation of pre-existing detrital chlorite grains, cracking parallel to the basal planes, and precipitation of

Table 2. Measured aspect ratios for the chlorite–mica aggregates and calculated values for s_1 and Δ for grains having initial aspect ratios of 1.25:1, 1.5:1, 2.0:1 and 2.5:1

	Ax. Rat. (measured)			s_1				$\Delta = s_1 s_3 - 1$			
Sample	$\frac{a_f}{b_f}$	$\frac{b_f}{c_f}$	$\frac{a_f}{c_f}$	$\frac{a_i}{c_i} = 1.25$	$\frac{a_i}{c_i} = 1.5$	$\frac{a_i}{c_i} = 2.0$	$\frac{a_i}{c_i} = 2.5$	$\frac{a_i}{c_i} = 1.25$	$\frac{a_i}{c_i} = 1.5$	$\frac{a_i}{c_i} = 2.0$	$\frac{a_i}{c_i} = 2.5$
SX-50	2.38	3.47	8.26	2.97	3.57	4.76	5.95	−0.142	0.0285	0.371	0.714
SX-68	2.96	2.63	7.78	3.70	4.44	5.92	7.40	0.409	0.688	1.25	1.81
SX-70	3.08	2.30	7.09	3.84	4.62	6.16	7.70	0.671	1.007	1.68	2.34
SX-71	2.91	3.02	8.78	3.63	4.36	5.82	7.27	0.205	0.446	0.928	1.41
SX-80	4.03	3.09	12.45	5.04	6.04	8.06	10.07	0.630	0.956	1.61	2.26

secondary chlorite and muscovite in the open cracks. Implications of this study are:

(1) Fracturing may play an important role in aggregate nucleation and growth. In addition, because the stress field is hydrostatic within an open fracture, differential stress plays no role in determining the crystallographic orientation in which secondary minerals grow; these secondary minerals are likely to nucleate on and maintain crystallographic continuity with similar minerals in the wall of the crack.

(2) Microprobe analyses, particularly in the detrital grains, clearly show two distinct chlorite compositions, with the high Mg end-member similar in composition to secondary chlorites that define the cleavage. This supports the interpretation of a primary-and-secondary origin for chlorite–mica aggregates.

(3) Despite the top-to-the-northwest noncoaxial strain experienced in the matrix of these rocks, deformation of the aggregates was largely coaxial, with extension always occurring nearly orthogonal to (001), as shown by the observation that the aggregates are longest normal to the basal planes. Thus, noncoaxial strain in the matrix is accommodated by a spinning coaxial deformation in the aggregates (e.g. Lister & Williams 1983).

(4) The final geometries of the aggregates (either slightly prolate or slightly oblate) suggests that extension parallel to x was also accompanied by shortening parallel to z, but with an overall volume gain for the aggregates. Thus, growth of the aggregates was strain induced.

Acknowledgements—This work was completed as part of B. Clark's Ph.D. thesis at The Pennsylvania State University. We would like to thank D. Anastasio, E. Beutner, T. Engelder, D. Kerrick and S. Shank for their helpful discussions, and R. Allmendinger for the use of 'Stereonet'. Thanks to C.-Y. Lu, Y.-C. Chan and others at National Taiwan University and W.-C. Lai from National Cheng Kung University for their logistical support, and to B. A. van der Pluijm and D. Aerden for their thorough reviews and helpful comments. Primary support for this work was provided by grants EAR-8904989 and EAR-9206560 from the National Science Foundation (to D. Fisher). Additional support was provided by a Williams/Scholten/Wright Scholarship from The Pennsylvania State University Department of Geosciences, Geological Society of America Grant number 4847-91, and a Sigma Xi Grant-in-Aid of Research to B. Clark.

REFERENCES

Attewell, P. B. & Taylor, R. K. 1969. A microtextural interpretation of a Welsh slate. *Int. J. Rock Mech. Mining Sci.* **6**, 423–438.

Behre, C. H., Jr. 1933. Slate in Pennsylvania. *Bull. geol. Surv. Penn.* **M16**, 1–400.

Bell, T. H. 1981. Foliation development—the contribution, geometry and significance of progressive, bulk, inhomogeneous shortening. *Tectonophysics* **75**, 273–296.

Bell, T. H. & Johnson, S. E. 1989. Porphyroblast inclusion trails: the key to orogenesis. *J. metamorph. Geol.* **7**, 279–310.

Bell, T. H., Johnson, S. E., Davis, B., Forde, A., Hayward, N. & Wilkins, C. 1992. Porphyroblast inclusion-trail orientation data: eppure non son girate! *J. metamorph. Geol.* **10**, 295–307.

Bell, T. H., Rubenach, M. J. & Fleming, P. D. 1986. Porphyroblast nucleation, growth and dissolution in regional metamorphic rocks as a function of deformation partitioning during foliation development. *J. metamorph. Geol.* **4**, 37–67.

Beutner, E. C. 1978. Slaty cleavage and related strain in Martinsburg Slate, Delaware Water Gap, New Jersey. *Am. J. Sci.* **278**, 1–23.

Beutner, E. C. & Diegel, F. A. 1985. Determination of fold kinematics from syntectonic fibers in pressure shadows, Martinsburg slate, N. J. *Am. J. Sci.* **285**, 16–50.

Beutner, E. C., Fisher, D. M. & Kirkpatrick, J. L. 1988. Kinematics of deformation at a thrust fault ramp (?) from syntectonic fibers in pressure shadows. In: *Geometries and Mechanisms of Thrusting, With Special Reference to the Appalachians* (edited by Mitra, G. & Wojtal, S.). *Spec. Pap. geol. Soc. Am.* **222**, 77–88.

Clark, M. B., Fisher, D. M., Lu, C.-Y. & Chen, C.-H. 1993. Kinematic analyses of the Hsüehshan Range, Taiwan: a large-scale pop-up structure. *Tectonics* **12**, 205–217.

Chen, C.-H. 1984. Determination of lower greenschist facies boundary by K–mica–chlorite crystallinity in the Central Range, Taiwan. *Proc. geol. Soc. China* **27**, 41–53.

Craig, J., Fitches, W. R. & Maltman, A. J. 1982. Chlorite–mica stacks in low-strain rocks from central Wales. *Geol. Mag.* **119**, 243–256.

Davis, D., Suppe, J. & Dahlen, F. A. 1983. Mechanics of fold-and-thrust belts and accretionary wedges. *J. geophys. Res.* **88**, 1153–1172.

Durney, D. W. & Ramsay, J. G. 1973. Incremental strains measured by syntectonic crystal growths. In: *Gravity and Tectonics* (edited by DeJong, K. & Sholten, R.). John Wiley and Sons, New York, 67–96.

Ellis, M. 1986. The determination of progressive deformation histories from antitaxial syntectonic crystal fibres. *J. Struct. Geol.* **8**, 701–709.

Ernst, W. G., Ho, C. S. & Liou, J. G. 1988. Rifting, drifting, and crustal accretion in the Taiwan sector of the Asiatic continental margin. In: *Tectonostratigraphic Terranes of the Circum-Pacific Region. Circum-Pacific Council for Energy and Mineral Resources: Earth Science Series* (edited by Howell, D. G.). 375–389.

Erslev, E. A. & Ge, H. 1990. Least-squares center-to-center and mean object ellipse fabric analysis. *J. Struct. Geol.* **12**, 1047–1059.

Fisher, D. M. 1990. Orientation history and rheology in slates, Kodiak and Afognak Islands, Alaska. *J. Struct. Geol.* **12**, 483–498.

Flinn, D. 1962. On folding during three dimensional progressive deformation. *Q. Jl. geol. Soc. Lond.* **118**, 385–428.

Gregg, W. J. 1986. Deformation of chlorite–mica aggregates in cleaved psammitic and pelitic rocks from Islesboro, Maine, U.S.A. *J. Struct. Geol.* **8**, 59–68.

Ho, C. S. 1975. *An Introduction to the Geology of Taiwan—Explanatory Text of the Geologic Map of Taiwan.* Ministry of Economic Affairs, Taipei, Taiwan, Republic of China.

Ho, C. S. 1986. A synthesis of the geologic evolution of Taiwan. *Tectonophysics* **125**, 1–16.

Ho, C. S. 1988. *An Introduction to the Geology of Taiwan—Explanatory Text of the Geologic Map of Taiwan, 2nd ed.* Ministry of Economic Affairs, Taipei, Taiwan, Republic of China.

Li, G., Peacor, D. R., Merriman, R. J., Roberts, B. & van der Pluijm, B. A. 1994. TEM and AEM study of the origin of chlorite–mica stacks in slates: an example from central Wales, U.K. *J. Struct. Geol.* **16**, 1139–1157.

Lister, G. S. & Williams, P. F. 1983. The partitioning of deformation in flowing rock masses. *Tectonophysics* **92**, 1–33.

Lister, G. S., Boland, J. N. & Zwart, H. J. 1986. Step-wise growth of biotite porphyroblasts in pelitic schists of the western Lys-Caillaouas massif (Pyrenees). *J. Struct. Geol.* **8**, 543–562.

Ramsay, J. G. & Huber, M. I. 1983. *The Techniques of Modern Structural Geology, Volume 1: Strain Analysis.* Academic Press, London.

Sorby, H. C. 1853. On the origin of slaty cleavage. *Edinburgh New Philos. J.* **55**, 137–148.

Stanley, R. S., Hill, L. B., Chang, H. C. & Hu, H. N. 1981. A transect through the metamorphic core of the Central Mountains, Taiwan. *Mem. geol. Soc. China* **4**, 443–473.

van der Pluijm, B. A. & Kaars-Sijpesteijn, C. H. 1984. Chlorite–mica aggregates: morphology, orientation, development and bearing on cleavage formation in very-low-grade rocks. *J. Struct. Geol.* **6**, 399–407.

Vernon, R. H. 1977. Microfabric of mica aggregates in partly recrystallized biotite. *Contr. Miner. Petrol.* **61**, 175–185.

Voll, G. 1960. New work on petrofabrics. *Lpool Mnchr Geol. J.* **2**, 503–597.

Weber, K. 1981. Kinematic and metamorphic aspects of cleavage development in selected slates. *Tectonophysics* **78**, 291–306.

White, S. H. & Knipe, R. J. 1978. Microstructure and cleavage development in selected slates. *Contr. Miner. Petrol.* **66**, 165–174.

Wickham, J. S. 1973. An estimate of strain increments in a naturally deformed carbonate rock. *Am. J. Sci.* **273**, 23–47.

Williams, P. J. & Schoneveld, C. 1981. Garnet rotation and the development of axial plane crenulation cleavage. *Tectonophysics* **78**, 307–334.

Woodland, B. G. 1982. Gradational development of domainal slaty cleavage, its origin and relation to chlorite porphyroblasts in the Martinsburg Formation, eastern Pennsylvania. *Tectonophysics* **82**, 89–124.

Woodland, B. G. 1985. Relationship of concretions and chlorite–muscovite porphyroblasts to the development of domainal cleavage in low-grade metamorphic deformed rocks from north-central Wales, Great Britain. *J. Struct. Geol.* **7**, 205–215.